



PCCP

Counterintuitive Torsional Barriers Controlled by Hydrogen Bonding

Journal:	<i>Physical Chemistry Chemical Physics</i>
Manuscript ID	CP-ART-06-2020-003285.R1
Article Type:	Paper
Date Submitted by the Author:	14-Aug-2020
Complete List of Authors:	Barbero, Héctor; Ohio University Meunier, Antoine; Ohio University Kotturi, Kondalarao; Ohio University, Chemistry and Biochemistry Smith, Ashton; Ohio University Kyritsakas, Nathalie; University of Strasbourg Killmeyer, Adam; Ohio University Rabbani, Ramin; Ohio University Nazimuddin, Md; Ohio University Masson, Eric; Ohio University

SCHOLARONE™
Manuscripts

ARTICLE

Counterintuitive Torsional Barriers Controlled by Hydrogen Bonding

Received 00th January 20xx,
Accepted 00th January 20xx

Héctor Barbero,^a Antoine Meunier,^a Kondalarao Kotturi,^a Ashton Smith,^a Nathalie Kyritsakas,^b Adam Killmeyer,^a Ramin Rabbani,^a Md Nazimuddin^a and Eric Masson*

DOI: 10.1039/x0xx00000x

The torsional barriers along the C_{aryl}-C_{aryl} axis of a pair of isosteric disubstituted biphenyls were determined by variable temperature ¹H NMR spectroscopy in three solvents with contrasted hydrogen bond accepting abilities (1,1,2,2-tetrachloroethane-d², nitrobenzene-d⁵ and dimethyl sulfoxide-d⁶). One of the biphenyl scaffolds was substituted at its *ortho* and *ortho'* positions with *N'*-acylcarbohydrazide groups that could engage in a pair of intramolecular NH/O=C hydrogen bonding interactions at the ground state, but not at the transition state of the torsional isomerization pathway. The torsional barrier of this biphenyl was exceedingly low despite the presence of the hydrogen bonds (16.1, 15.6 and 13.4 kcal/mol in the three aforementioned solvents), compared to the barrier of the reference biphenyl (15.3 ± 0.1 kcal/mol on average). Density functional theory and the solvation model developed by Hunter were used to decipher the various forces at play. They highlighted the strong stabilization of hydrogen bond donating solutes not only by hydrogen bond accepting solvents, but also by weakly polar, yet polarizable solvents. As fast exchanges on the NMR time scale were observed above the melting point of dimethyl sulfoxide-d⁶, a simple but accurate model was also proposed to extrapolate low free activation energies in a pure solvent (dimethyl sulfoxide-d⁶) from higher ones determined in mixtures of solvents (dimethyl sulfoxide-d⁶ in nitrobenzene-d⁵).

Introduction

The notion of hydrogen bonding is ubiquitous in the chemical literature and is being taught at both undergraduate and graduate levels with varying degrees of simplification or sophistication.^{1–5} Hydrogen bonding is also responsible for the formation of landmark host-guest complexes,^{6–11} such as the Hamilton receptor and barbiturates.¹² As part of a study that evaluates the impact of substituents on the torsional barriers of biphenyls,^{13–16} we identified an intriguing intramolecular hydrogen bonding pattern in biphenyls substituted with *N'*-acylcarbohydrazides at their *ortho* and *ortho'*-positions. An X-ray diffraction structure of biphenyl **1** crystallized in 1,1,2,2-tetrachloroethane-d² shows a pair of intramolecular hydrogen bonds between the NHα donors and the *N'*-acyl acceptors of the opposite *ortho*-substituents (see Figure 1). Relative to an isosteric system like biphenyl **2** that does not engage in such interactions (see Figure 1), we suspected first that the pair of hydrogen bonds would significantly slow down the rotation along the C_{aryl}-C_{aryl} axis. Those would have to be disrupted at the transition state of the isomerization where both aryl units are

close to coplanar. We show here that the behavior of simple scaffolds such as these can be deceptive, and that our assumption was incorrect. We provide a detailed justification for the counterintuitive free energies of torsion we measured in three solvents with contrasted hydrogen bond accepting properties, 1,1,2,2-tetrachloroethane-d² (TCE-d²), nitrobenzene-d⁵ (PhNO₂-d⁵) and dimethylsulfoxide-d⁶ (DMSO-d⁶; -dⁿ suffix omitted later for clarity), and in a mixture of the last two solvents. The three solvents were chosen as they dissolve biphenyls **1** and **2** at millimolar concentrations and cover a wide range of hydrogen bond accepting ability and polarity. TCE is a very poor H-bond acceptor (Hunter's β parameter is 1.3)¹⁷ and is a weakly polar solvent (dielectric constant ε = 8.4).^{18,19} PhNO₂ and DMSO are moderate and very strong H-bond acceptors, respectively (β = 3.7 and 8.9)¹⁷ and are both much more polar than TCE (ε = 35 and 47, respectively).^{18,19}

Results and Discussion

Synthesis and X-ray diffraction structures

Biphenyl **1** was prepared from biphenyl-2,2'-dicarboxylic acid and isobutyric acid hydrazide in 65% yield over two steps. Biphenyl **2** was obtained from 2-iodoacetophenone in 3 steps (38% overall yield), after α-bromination of the acetyl unit,²⁰ substitution with cesium isobutyrate,²¹ and an Ullmann-type coupling promoted by copper(I)-thiophene-2-carboxylate (see SI section for details).^{22,23} The X-ray diffraction structure of

^a Department of Chemistry and Biochemistry, Ohio University, Athens, Ohio 45701, United States.

^b Molecular Tectonics Laboratory, University of Strasbourg, UMR UDS-CNRS 7140, Institut le Bel, F-67000 Strasbourg, France.

Electronic Supplementary Information (ESI) available: preparation and characterization of scaffolds **1** – **3** and precursors; variable temperature ¹H NMR experiments, computational details, X-ray crystallographic analysis. CCDC 2004107, 2004108. For crystallographic data in CIF format, see DOI: 10.1039/x0xx00000x.

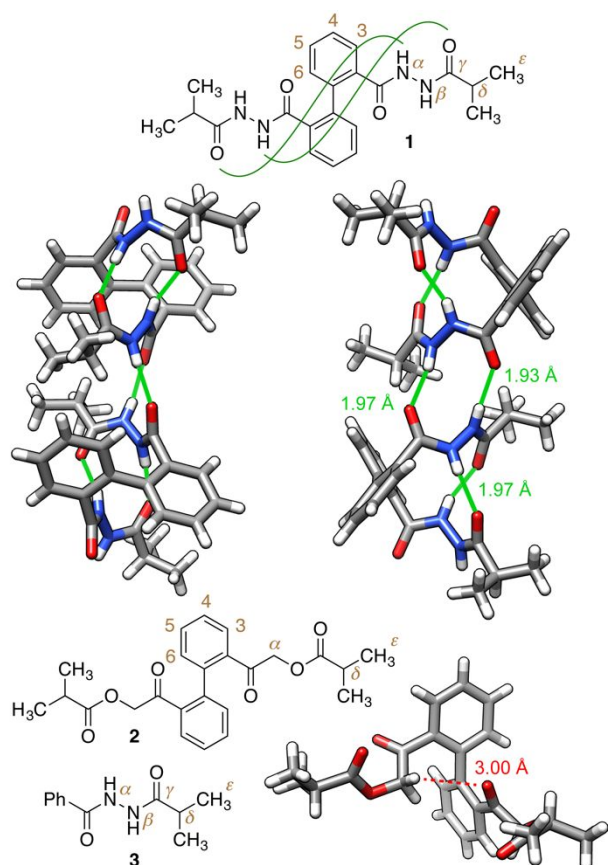


Figure 1. X-ray diffraction structures of biphenyls **1** (two views) and **2**; reference *N'*-acylhydrazide **3**. Intra- and intermolecular hydrogen bonds are highlighted in green.

biphenyl **1** shows a C(2)-C(1)-C(1')-C(2') dihedral angle of 109.8°, N-H α ...O=C γ hydrogen bond lengths of 1.97 Å, and H α -O=C γ angles of 131° and 135°, respectively (see Figure 1 for numbering). Hydrogens NH β engage in intermolecular hydrogen bonding with the benzoyl groups of neighboring biphenyl units (1.93 and 1.97 Å, see Figure 1). Biphenyl **2** was crystallized in a mixture of hexane and ethyl acetate; the X-ray crystal structure does not show any significant interaction between the *ortho* and *ortho'*-substituents. The closest contact is measured between the benzoyl unit of one chain and the α -methylene group of the other chain, with the shortest CH...O distances being 3.00 Å (see Figure 1).

Determination of the torsional barriers by nuclear magnetic resonance spectroscopy

The isopropyl substituents, with their diastereotopic pair of methyl groups, were chosen as probes to monitor the rates of torsional isomerization k of biphenyls **1** and **2** using variable temperature ^1H NMR spectroscopy and spectral line fitting (see Figure 2 and SI section). In the case of biphenyl **2**, the hydrogen atoms of the α -methylene group are also diastereotopic and can be used for the same purpose (see SI section). From Eyring equation (1), enthalpies ΔH^\ddagger , entropies ΔS^\ddagger and free energies of activation ΔG^\ddagger can be extracted from a plot of $\ln k/T$ as a function of $1/T$ (see Figure 3). The activation enthalpies and entropies are readily extracted from the slopes of the best

straight lines and their intersection with the y-axis, respectively (see equation 2), as long as these two parameters are considered temperature independent.

$$k = \frac{k_B T}{h} e^{-\Delta G^\ddagger/RT} \quad (1)$$

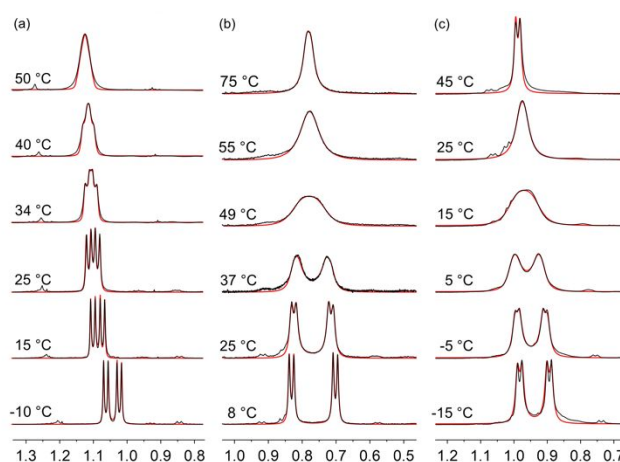


Figure 2. ^1H NMR signals of the isopropyl substituent in biphenyl **1** (H^β ; see Figure 1 for numbering) as a function of temperature in (a) TCE- d^2 , (b) PhNO $_2$ - d^5 and (c) a 1.6 M DMSO- d^6 solution in PhNO $_2$ - d^5 . Line shape fitting in red.

$$\ln \frac{k}{T} = \frac{1}{T} \cdot \frac{-\Delta H^\ddagger}{R} + \left(\frac{\Delta S^\ddagger}{R} + \ln \frac{k_B}{h} \right) \quad (2)$$

Line fitting (see Figure 2, red traces) afforded free energies of torsion $\Delta G_{\text{TCE}}^\ddagger(\mathbf{1}) = 16.1 \pm 0.1$ kcal/mol, $\Delta G_{\text{PhNO}_2}^\ddagger(\mathbf{1}) = 15.6 \pm 0.1$ kcal/mol, $\Delta G_{\text{TCE}}^\ddagger(\mathbf{2}) = 15.4 \pm 0.2$ kcal/mol and $\Delta G_{\text{PhNO}_2}^\ddagger(\mathbf{2}) = 15.2 \pm 0.2$ kcal/mol, all calculated at 25 °C. Enthalpic and entropic contributions are listed in Table 1 and discussed later. Considering the pair of intramolecular H-bonds in the crystal structure of biphenyl **1**, we expected its torsional barriers to be significantly higher than reference biphenyl **2**. To the contrary the differences were just 0.7 and 0.4 kcal/mol in TCE and PhNO $_2$, respectively.

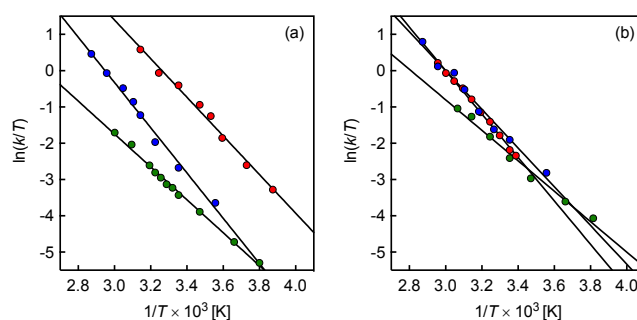


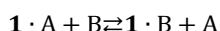
Figure 3. Rates of torsional isomerization, as obtained by line-fitting of ^1H NMR spectra, of (a) biphenyl **1** recorded at different temperatures, in TCE- d^2 (green dots), PhNO $_2$ - d^5 (blue dots) and a 1.6 M DMSO- d^6 solution in PhNO $_2$ - d^5 (red dots); (b) biphenyl **2** in TCE- d^2 (green dots), PhNO $_2$ - d^5 (blue dots) and DMSO- d^6 (red dots).

To assess the impact of a solvent that would possibly disrupt all H-bonds, we tried to determine the torsional free energies of both biphenyls in DMSO. Activation parameters for reference biphenyl **2** (see Table 1) were obtained by variable temperature ^1H NMR experiments, as described earlier. The free energy of

torsion $\Delta G_{\text{DMSO}}^{\ddagger}(2)$ was 15.3 ± 0.1 kcal/mol, similar to the barriers measured in TCE and PhNO₂.

With biphenyl **1**, however, fast exchange on the NMR time scale was observed above the melting point of the solvent (20 °C), thereby precluding an accurate determination of the torsional barrier. To circumvent this problem, we determined the torsional barriers of biphenyls **1** in PhNO₂ in the presence of increasing amounts of DMSO, and we propose here a simple model to extrapolate the torsional barrier in pure DMSO.

We considered the simple equilibrium between biphenyl **1** that interacts with two competing solvents A (PhNO₂) and B (DMSO). This equilibrium was also proposed by Hunter and coworkers to quantify hydrogen bonding interactions in mixtures of solvents.²⁴



The equilibrium constant K is obtained from equation 3.

$$K = \frac{[\mathbf{1} \cdot \text{B}][\text{A}]}{[\mathbf{1} \cdot \text{A}][\text{B}]} = \frac{x}{(1-x)} \frac{[\text{A}]}{[\text{B}]} \quad (3)$$

where x is the fraction of biphenyl **1** interacting with solvent B. Fraction x is thus obtained from equation 4.

$$x = \frac{K[\text{B}]}{K[\text{B}] + [\text{A}]} \quad (4)$$

The torsional barrier of biphenyl **1** in the mixture of solvents A and B can be easily determined at coalescence temperature with Eyring equation (1), from the corresponding rate of isomerization (see equation 5).

$$k = \frac{\pi \Delta \nu}{\sqrt{2}} \quad (5)$$

where $\Delta \nu$ is the difference in resonance frequencies of the diastereotopic nuclei in a slow exchange regime. Our hypothesis is that the torsional barrier ΔG^{\ddagger} , at coalescence temperature, is the average of the barriers in the pure solvents $\Delta G_{\text{A}}^{\ddagger}$ and $\Delta G_{\text{B}}^{\ddagger}$, weighted by the fractions of biphenyl **1** interacting with solvents A and B (see equations 6 and 7). In an ideal mixture of two solvents, the concentration of solvent A can be obtained from the concentration of solvent B, the molar masses of both solvents M_{A} and M_{B} , and the density of both solvents (ρ_{A} and ρ_{B} ; see equation 8 and SI section for details).

$$\Delta G^{\ddagger} = x \cdot \Delta G_{\text{B}}^{\ddagger} + (1-x) \cdot \Delta G_{\text{A}}^{\ddagger} \quad (6)$$

$$\Delta G^{\ddagger} = \frac{K[\text{B}] \cdot \Delta G_{\text{B}}^{\ddagger} + [\text{A}] \cdot \Delta G_{\text{A}}^{\ddagger}}{K[\text{B}] + [\text{A}]} \quad (7)$$

$$[\text{A}] = \frac{\rho_{\text{A}}}{M_{\text{A}}} - [\text{B}] \frac{\rho_{\text{A}} M_{\text{B}}}{\rho_{\text{B}} M_{\text{A}}} \quad (8)$$

Fitting ΔG^{\ddagger} as a function of $[\text{B}]$ (DMSO) would afford the torsional barrier $\Delta G_{\text{B}}^{\ddagger}$ in pure DMSO at a hypothetical (unknown) coalescence temperature.

To extrapolate a torsional barrier in pure DMSO at a *reference temperature* (25 °C), the free energies of activation in equation 7 must be expanded into their enthalpic and entropic contributions (see equation 9; T_{c} is the coalescence temperature at a given concentration of DMSO).

$$\Delta G^{\ddagger} = \frac{K[\text{B}] \cdot \Delta H_{\text{B}}^{\ddagger} + [\text{A}] \cdot \Delta H_{\text{A}}^{\ddagger}}{K[\text{B}] + [\text{A}]} - T_{\text{c}} \frac{K[\text{B}] \cdot \Delta S_{\text{B}}^{\ddagger} + [\text{A}] \cdot \Delta S_{\text{A}}^{\ddagger}}{K[\text{B}] + [\text{A}]} \quad (9)$$

One can then show that within the range of temperatures used in these NMR experiments, the coalescence temperature T_{c} varies linearly with the free energy of torsion ΔG^{\ddagger} (see the insert in Figure 4 and the SI section for details on this approximation). Therefore equation (10) can be used to extrapolate coalescence temperatures as a function of the concentration of DMSO and is used to substitute T_{c} in equation 9.

$$T_{\text{c}} = \frac{K'[\text{B}] \cdot T_{\text{B}} + [\text{A}] \cdot T_{\text{A}}}{K[\text{B}] + [\text{A}]} \quad (10)$$

where T_{A} and T_{B} are the coalescence temperatures of biphenyl **1** in pure solvents A and B, respectively, and K' is approximately equal to equilibrium constant K . A (virtual) coalescence temperature of -20.5 ± 0.8 °C for biphenyl **1** in pure DMSO was extrapolated from the fit at $[\text{B}] = 14.1$ M ($[\text{A}] = 0$; see red series (a) in Figure 4 and the orange dot at $T_{\text{c}} = 252.8$ K). 14.1 M is the concentration of DMSO-*d*⁶ in pure DMSO-*d*⁶. The remarkable precision of the fit shows that our rudimentary competitive solvation model, in which biphenyl **1** and its transition state are essentially solvated by microheterogeneous shells of only one solvent molecule (A or B), is adequate enough to extract the torsional barriers.

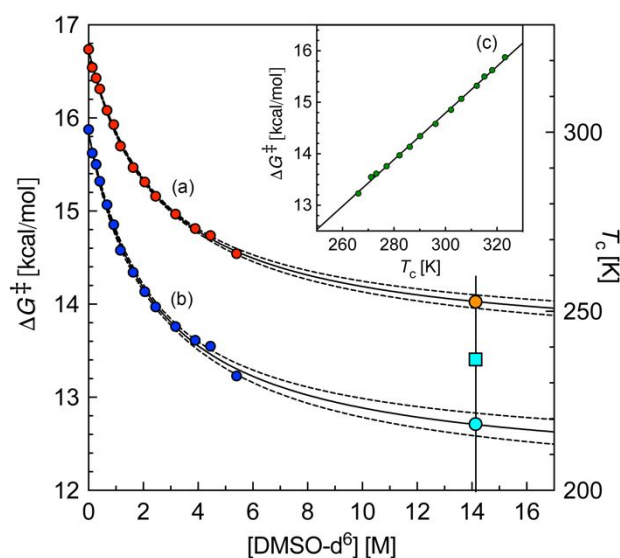


Figure 4. (a) Coalescence temperatures of the isopropyl ¹H NMR signal as a function of DMSO-*d*⁶ concentration in PhNO₂-*d*⁵, fitted using equation 10 (right y-axis). The orange dot corresponds to the virtual coalescence temperature in pure DMSO-*d*⁶ (−20.5 °C). (b) Free activation energy for the torsional isomerization of biphenyl **1** along its C_{aryl}-C_{aryl} axis, as a function of DMSO-*d*⁶ concentration, and fitted using equations 9 and 10 (left y-axis). The cyan dot and square correspond to the free energy of torsion in pure DMSO-*d*⁶ at the extrapolated, virtual coalescence temperature (−20.5 °C) and at 25 °C, respectively. Dotted lines represent 95% confidence intervals. (c) Linear correlation between coalescence temperatures T_{c} and free activation energies.

The activation enthalpies and entropies in pure DMSO (and therefore the free energy of torsion at any temperature) can now be obtained by fitting the measured free energies as a function of DMSO concentration, using equations 9 and 10. However, this would require fitting three parameters (K , $\Delta H_{\text{B}}^{\ddagger}$ and $\Delta S_{\text{B}}^{\ddagger}$) and would generate significant errors. Instead, we determined the enthalpies and entropies of torsion of biphenyl **1** in a 12% solution of DMSO in PhNO₂ ($\Delta H_{\text{AB}}^{\ddagger}$ and $\Delta S_{\text{AB}}^{\ddagger}$; $c_{\text{A}} = 8.7$ M; $c_{\text{B}} = 1.6$ M) by line-fitting of the relevant ¹H NMR signals, as described above (see Figure 2c and Figure 3a, red series). Rearranging the enthalpic term in equation 11 affords the enthalpy of torsion in pure DMSO ($\Delta H_{\text{B}}^{\ddagger}$, see equation 12).

$$\Delta H_{\text{AB}}^{\ddagger} = \frac{Kc_{\text{B}} \cdot \Delta H_{\text{B}}^{\ddagger} + c_{\text{A}} \cdot \Delta H_{\text{A}}^{\ddagger}}{Kc_{\text{B}} + c_{\text{A}}} \quad (11)$$

$$\Delta H_{\text{B}}^{\ddagger} = \frac{(Kc_{\text{B}} + c_{\text{A}}) \cdot \Delta H_{\text{AB}}^{\ddagger} - c_{\text{A}} \cdot \Delta H_{\text{A}}^{\ddagger}}{Kc_{\text{B}}} \quad (12)$$

A similar relationship can be used for the entropic term $\Delta S_{\text{B}}^{\ddagger}$, and equations 9 and 10 could then be applied to fit free activation energies as a function of DMSO concentration with only one unknown parameter (equilibrium constant K). However, we prefer to fit parameter $\Delta S_{\text{B}}^{\ddagger}$ also, as a lower error is obtained with this method. The fit is again remarkably precise (see Figure 4, blue series b), thereby confirming the validity of our model.

All activation parameters of biphenyl **1** are presented in Table 1. From the enthalpies and entropies of activation in pure DMSO ($\Delta H_{\text{B}}^{\ddagger} = 8.8 \pm 1.1$ kcal/mol and $\Delta S_{\text{B}}^{\ddagger} = 15 \pm 2$ cal/molK), free energies of torsion at the virtual -20.5 °C coalescence temperature and at 25 °C are 12.7 ± 0.1 and 13.4 ± 0.1 kcal/mol, respectively (see cyan dot and square in Figure 4). The torsional barrier is thus 2.7 and 2.2 kcal/mol lower in DMSO than in TCE and PhNO₂ at 25 °C, respectively ($\Delta G_{\text{TCE}}^{\ddagger}(\mathbf{1}) = 16.1 \pm 0.1$ kcal/mol and $\Delta G_{\text{PhNO}_2}^{\ddagger}(\mathbf{1}) = 15.6 \pm 0.1$ kcal/mol, see Table 1).

Table 1. Kinetic parameters for the torsional isomerization of biphenyls **1** and **2** in TCE-d², PhNO₂-d⁵ and DMSO-d⁶.

	TCE-d ²	PhNO ₂ -d ⁵	DMSO-d ⁶
T_c^a	323	323	252.7 ± 0.8
$\Delta H^{\ddagger b}$	9.0 ± 0.2	12.4 ± 0.5	8.8 ± 1.1
1 $\Delta S^{\ddagger c}$	-24 ± 1	-11 ± 2	-15 ± 2
ΔG^{\ddagger} at T_c^b	16.7 ± 0.1	15.9 ± 0.1	12.7 ± 0.1
ΔG^{\ddagger} at 25 °C ^b	16.1 ± 0.1	15.6 ± 0.1	13.4 ± 0.1
T_c^a	323	322	322
$\Delta H^{\ddagger b}$	8.3 ± 0.4	10.6 ± 0.5	11.9 ± 0.2
2 $\Delta S^{\ddagger c}$	-24 ± 1	-15 ± 2	-12 ± 1
ΔG^{\ddagger} at T_c^b	16.0 ± 0.2	15.6 ± 0.2	15.6 ± 0.1
ΔG^{\ddagger} at 25 °C ^b	15.4 ± 0.2	15.2 ± 0.2	15.3 ± 0.1

^a Coalescence temperature in K. ^b in kcal/mol. ^c in cal/molK.

Two seemingly counterintuitive conclusions emerge from these results: (1) the torsional barrier of isosteric biphenyls **1** and **2** are very similar in TCE and PhNO₂, while we expected a much slower rotation for intramolecularly H-bonded biphenyl **1**; and

(2) biphenyl **1** rotates 26 (± 5) times *faster* than biphenyl **2** in DMSO at 25 °C (the barrier being 1.9 (± 0.1) kcal/mol lower).

Determination of the torsional barriers *in silico* and rationalization

To decipher the mechanism behind these kinetic parameters, we tried to reproduce them *in silico* using density functional theory (DFT) calculations. Those allow us to split the torsional barriers into three components: (1) the electronic gas phase contribution to the barrier ΔE^{\ddagger} (at 0 K), (2) the thermal correction ΔG_T^{\ddagger} obtained from the enthalpic (ΔH_T^{\ddagger}) and entropic ($-T\Delta S_T^{\ddagger}$) contributions at higher temperatures, and (3) solvation contributions $\Delta G_{\text{solv}}^{\ddagger}$ (see equation 13).

$$\Delta G^{\ddagger} = \Delta E^{\ddagger} + \Delta G_T^{\ddagger} + \Delta G_{\text{solv}}^{\ddagger} \quad (13)$$

We present here the three most stable ground state conformers of biphenyl **1** with zero, one, and two intramolecular hydrogen bonding interactions, and the lowest energy transition state of the torsional isomerization, calculated with the B3LYP functional and def2-TZVP basis sets in the gas phase (see Figure 5, structures **1a** – **1c** and **1^{TS}**). As expected, transition state **1^{TS}** is void of any hydrogen bonding interaction. Structures **2a** – **2c**, which mimic conformers **1a** – **1c** and are also local energy minima, are shown in Figure 6. Details for the choice of the B3LYP functional are given later. The X-ray crystal structures of biphenyls **1** and **2** closely resemble conformers **1c** (with two intramolecular hydrogen bonds, see Figure 5), and **2b** (with one mid-range CH-O interaction, see Figure 6), respectively; overlapped structures are presented in the SI section. We also verified that biphenyls **1** and **2** are indeed isosteric; we found that the molecular volumes of conformers **1c** and **2c** (delimited by a 0.001 electron/Bohr³ isodensity surface) are identical (541 Å³).

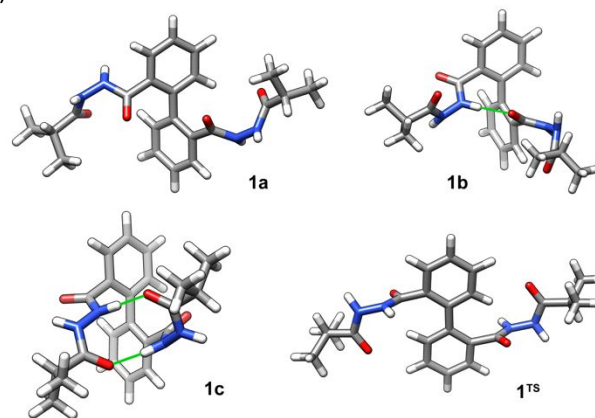


Figure 5. Lowest energy conformers of biphenyl **1** with 0, 1 and 2 intramolecular hydrogen bonds (**1a** – **1c**, respectively), and the lowest energy transition state along the C_{aryl}-C_{aryl} torsion pathway (**1^{TS}**). Hydrogen bonds are highlighted in green.

Torsional barriers that are closest to those determined experimentally were obtained by calculating the electronic gas phase energies of the B3LYP-optimized structures with Truhlar's M05-2X functional.²⁵ The choice of functional is again discussed later. When comparing electronic contributions in the gas phase, conformer **1c**, with its two intramolecular hydrogen bonds, is more stable than conformers **1a** and **1b** by 10.1 and

7.3 kcal/mol, respectively (see Table 2). The electronic contribution to the torsional barrier ΔE^\ddagger (i.e. the energy difference between conformer **1c** and transition state **1^{TS}**) is 22.6 kcal/mol. Vibrational analysis at the B3LYP/def2-TZVP level afforded the enthalpic and entropic contributions to the stabilities of the ground and transition states (see SI section for details on methods and approximations). Remarkably, both the enthalpic and entropic corrections to the torsional barrier are insignificant ($\Delta H^\ddagger = -0.6$ kcal/mol and $T\Delta S^\ddagger = +0.4$ kcal/mol), thereby bringing the free energy of torsion to 21.6 kcal/mol in the gas phase. The near-zero entropic contribution to the torsion is likely caused by two competing factors: (1) a loss of flexibility in the biphenyl backbone at the transition state, and (2) a gain in flexibility upon disruption of the pair of intramolecular hydrogen bonds present in the ground state.

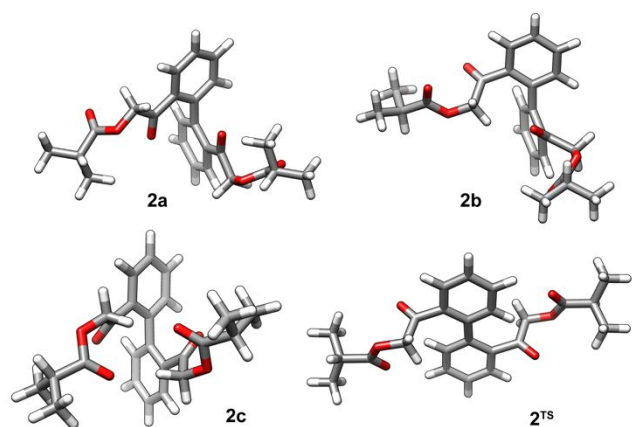


Figure 6. Three conformers biphenyl **2** mimicking those of biphenyl **1**. Lowest energy transition state along the $C_{\text{aryl}}-C_{\text{aryl}}$ torsion pathway (**2^{TS}**).

By comparison, the most stable conformer of biphenyl **2** is structure **2b**, which closely resembles the X-ray structure (see Figure 1). Although electronic contributions favor “wrapped” conformer **2c** by 1.6 kcal/mol due to a pair of favorable CH–O interactions that mirror the NH–O hydrogen bonds in conformer **1c**, enthalpic and entropic contributions to the distribution of conformers reverse the trend. In the gas phase, conformer **2b** is more stable than structures **2a** and **2c** by 0.5 and 1.5 kcal/mol, respectively (see Table 2). The electronic contribution to the torsional barrier is 10.3 kcal/mol, starting from ground state conformer **2b**. While the enthalpic contribution ΔH^\ddagger is only -0.5 kcal/mol (similarly to biphenyl **1**), a significant entropic penalty is imposed during the torsion ($T\Delta S^\ddagger = -4.2$ kcal/mol). As discussed above for biphenyl **1**, the entropic penalty is expected, as the biphenyl backbone in transition state **2^{TS}** is significantly less flexible than in ground state **2b** (see Figure 6). The thermal correction thus brings the free energy of torsion in the gas phase to 14.0 kcal/mol.

As free energies of torsion from “wrapped” conformers **1c** and **2c** to their respective transition state are 21.6 and 12.5 kcal/mol, respectively, the strength of the pair of intramolecular hydrogen bonds in biphenyl **1c** can be estimated at 9.1 kcal/mol in the gas phase. A 7.9 kcal/mol difference is calculated for the

stabilities of conformers **1a** (with no intramolecular hydrogen bond) and **1c** (with the pair of hydrogen bonds). Both values could be used to quantify the strength of the double intramolecular hydrogen bond, as long as the reference (i.e. the non-H-bonded structure) is clearly defined.

Hunter proposed equation 14 to predict the strength of hydrogen bonds, where α_S and β_S are H-bond donor and acceptor parameters of the solvent, and α and β the H-bond donor and acceptor parameters of the solute.^{17,26,27} In this case, α_S and β_S equal 0 as biphenyl **1** is in the gas phase. Hunter showed that parameters α and β can be readily obtained from maximum and minimum electrostatic potentials generated by a positive point-charge on the van der Waals surface of the molecule at the semi-empirical AM1 level (see equations 15a and 15b). We found $\alpha = 2.8$ and $\beta = 5.8$ for the *N'*-acylcarbohydrazide group (see SI section for details on the calculation). These groups thus resemble amides for their H-bond donating abilities, but they are weaker H-bond acceptors ($\alpha = 2.9$ and $\beta = 8.3$ for amides).¹⁷

$$\Delta\Delta G_{\text{H-bond}} = -(\alpha - \alpha_S)(\beta - \beta_S) \quad (14)$$

$$\alpha = \frac{E_{\text{max}}}{52} \quad (15a) \quad \beta = \frac{-E_{\text{min}}}{52} \quad (15b)$$

Equation 14 returns an H-bond strength $\Delta\Delta G_{\text{H-bond}}$ of -3.9 kcal/mol per interaction, and hence 7.8 kcal/mol for the pair of hydrogen bonds in biphenyl **1c** if one neglects any cooperativity effect. This is in perfect agreement with the 7.9 kcal/mol stabilization obtained above! As depicted in Figure 5, the accuracy of this model confirms that the *N'*-acylcarbohydrazide groups do not undergo adverse conformational work when engaging in intramolecular hydrogen bonding.

Clearly, the free energies of torsion calculated in the gas phase vastly overestimate the barriers measured in solution for biphenyl **1** (by 5.3–8.2 kcal/mol depending on the solvent), and slightly underestimate those in biphenyl **2** (by 1.3 kcal/mol). These differences must therefore find their root in the free energies of solvation of the transition states relative to the ground states $\Delta G_{\text{solv}}^\ddagger$. We decided to calculate those using the COSMO-RS method^{28–31} developed by Klamt and coworkers and implemented in the COSMOtherm program³² (see SI section for additional computational details). Structures were reoptimized at the BP/TZVP level³¹ in the absence and presence of the COSMO²⁸ solvation term, and energies were refined at the BP/def2-TZVPD level, as COSMOtherm is parametrized to return the most accurate free energies of solvation when input solute geometries are optimized at those levels of theory. The solvation term is then added to the free energy of torsion calculated in the gas phase (see equation 13).

Despite being a poor H-bond acceptor, TCE stabilizes transition state **1^{TS}** better than the doubly H-bonded ground state conformer **1c** by 4.5 kcal/mol (see energy term $\Delta\Delta G_{\text{solv}}^{\text{rel}}$ in Table 2), thereby bringing the calculated torsional barrier in this

solvent down to 17.1 kcal/mol (within 1.0 kcal/mol of the experimental free energy of activation). TCE also stabilizes conformers **1a** and **1b** (with zero or one intramolecular H-bonding interaction) much better than conformer **1c** (by 3.4 and 4.2 kcal/mol, respectively). Doubly H-bonded conformer **1c** is thus barely favored over singly H-bonded conformer **1b** (by 0.6 kcal/mol, see Table 2). This illustrates that TCE can compete for hydrogen bonding interactions with the *N'*-acyl units of biphenyl **1**. The stabilization of transition state **1^{TS}** relative to conformer **1c** ($\Delta\Delta G_{\text{solv}}^{\text{rel}} = -4.5$ kcal/mol) by TCE can be readily approximated using Hunter's formalism and equation 16, with $\alpha_S = 1.4^{33}$ and $\beta_S = 1.3^{17}$. $\Delta\Delta G_{\text{solv}}^{\text{rel}}$ is -4.8 kcal/mol, again exceptionally close to our calculated relative solvation term $\Delta\Delta G_{\text{solv}}^{\text{rel}}$ (see Table 2).

$$\Delta\Delta G_{\text{solv}}^{\text{rel}} = 2[(\alpha - \alpha_S)(\beta - \beta_S) - \alpha\beta] = 2[\alpha_S\beta_S - \alpha\beta_S - \alpha_S\beta]$$

To the contrary, TCE stabilizes the most stable ground state conformer of biphenyl **2** (structure **2b**) just slightly better than transition state **2^{TS}** (1.4 kcal/mol), thereby increasing the calculated torsional barrier from 14.0 kcal/mol in the gas phase to 15.4 kcal/mol, exactly as determined experimentally.

We note that in the solid state, short distances are observed between selected atoms in TCE and biphenyl **1** (NH β ...Cl and C γ =O...Cl distances are 3.26 and 3.13 Å, respectively; see Figure S17 in the SI section). To rule out any unusual intermolecular interaction between biphenyl **1** and TCE as solvent, we reoptimized the biphenyl **1**/TCE pair starting from the X-ray diffraction geometry in conjunction with the COSMO-RS solvation model, at the B3LYP/def2-TZVP level. The distance between TCE and biphenyl **1** increased significantly (NH β ...Cl and C γ =O...Cl distances 3.64 and 3.54 Å, respectively). The short TCE/biphenyl **1** distances measured in the solid state are thus merely caused by crystal packing, and a continuum solvation model such as COSMO-RS can be safely used in our evaluation.

In PhNO₂, the solvation free energies of transition state **1^{TS}** and ground state conformer **1a** (or **1b**), are 6.2 and 4.8 kcal/mol higher than doubly H-bonded conformer **1c**, respectively. Conformers **1c** and **1b** are now equally stable (see Table 2). The calculated free energy of torsion thus decreases from 21.6 kcal/mol in the gas phase to 15.4 kcal/mol, within 0.2 kcal/mol of the experimental kinetic parameter. Equation 16 with $\alpha_S = 1.4$ and $\beta_S = 4.1^{34}$ returns -6.7 kcal/mol for $\Delta\Delta G_{\text{solv}}^{\text{rel}}$, again in excellent agreement with the calculated $\Delta\Delta G_{\text{solv}}^{\text{rel}}$ term (-6.2 kcal/mol, see Table 2). Like TCE, PhNO₂ barely affects the torsional barrier of biphenyl **2** (15.1 vs. 15.2 kcal/mol for calculated and experimental free energies of torsion, respectively).

As solvation has a major impact on the torsional barriers of biphenyl **1**, we tested whether an archetypically non-polar solvent like cyclohexane ($\epsilon = 2.0$, $\alpha_S = 0.4$ and $\beta_S = 0.6$, calculated from equations 15a and 15b)¹⁷ could also lower the torsional barrier in silico, compared to gas phase conditions. We found that cyclohexane solvates transition state **1^{TS}** better than

ground state conformer **1c** by -2.6 kcal/mol, again in good agreement with the $\Delta\Delta G_{\text{solv}}^{\text{rel}}$ term calculated using Hunter's formalism and equation 16 (-1.9 kcal/mol). This clearly illustrates that even a very poor H-bond acceptor and H-bond donor can solvate strong H-bond donors and acceptors like the N-H...O=C pair, via dipole-dipole interactions, but also via dipole-induced dipole interactions. Hunter's parameters calculated using equations 15a and 15b are purely electrostatic in nature, and do not include a polarizability term. This could cause the mild underestimation, if at all significant, of the relative solvation term $\Delta\Delta G_{\text{solv}}^{\text{rel}}$ compared to the one obtained from the COSMO-RS solvation model (0.7 kcal/mol). This conclusion is further supported by referring to Catalán's solvent polarizability scale SP.³⁵ The scale is based on the 0-0 component of the long wavelength $\pi \rightarrow \pi^*$ absorption band of a (16) styrene chromophore dissolved in solvents of interest. The chromophore is non-polar in both its ground and excited state, and therefore SP values are solely influenced by the polarizability, and not the polarity of the solvent. With the gas phase and carbon disulfide being used as references (SP = 0 and 1, respectively), the SP values of cyclohexane, TCE and PhNO₂ are 0.68, 0.77,³⁶ and 0.89, respectively; all three solvents are highly polarizable. While dipole-dipole interactions certainly dominate the solvation effects in TCE and PhNO₂, dipole-induced dipole interactions might play a modest role as well.

As DMSO is a much stronger H-bond acceptor than TCE and PhNO₂ ($\alpha_S = 0.8$ and $\beta_S = 8.9$),¹⁷ structures **1^{TS}**, **1a** and **1b** are much better solvated in this solvent than conformer **1c** by 12.2, 9.8 and 8.1 kcal/mol, respectively. This is in excellent agreement with Hunter's formalism that returns a $\Delta\Delta G_{\text{solv}}^{\text{rel}}$ term equal to -10.9 kcal/mol (see equation 16). If doubly H-bonded biphenyl **1c** were the most stable ground state conformer in DMSO, the torsional barrier would decrease from 21.6 kcal/mol in the gas phase to 9.4 kcal/mol in this solvent. However, disruption of at least one intramolecular hydrogen bond is now favorable in DMSO, and mono-H-bonded biphenyl **1b** becomes the most stable conformer (by 3.3 kcal/mol compared to conformer **1c**). This extra stabilization of the mono-H-bonded conformer brings the calculated torsional barrier to 12.7 kcal/mol (within 0.6 kcal/mol of the experimental kinetic parameter, see Table 1). Like TCE and PhNO₂, the impact of DMSO on the torsional barrier of biphenyl **2** is very mild (0.8 kcal/mol extra stabilization for the ground state), and the calculated barrier in that solvent is 14.9 kcal/mol (vs. 15.3 kcal/mol determined experimentally).

We found it surprising that DMSO would not disrupt both intramolecular hydrogen bonds in the ground state of biphenyl **1** (mono H-bonded conformer **1b** is 1.3 kcal/mol more stable than non-H-bonded conformer **1a**). To test this feature experimentally, we measured the chemical shift gradient of the NH signals as a function of temperature, and we compared those with control *N'*-acyl hydrazide **3** (that does not engage in intramolecular hydrogen bonding, see Figure 1). Significant differences in gradients between biphenyl **1** and control **3**

Table 2. Kinetic parameters calculated at the B3LYP/def2-TZVP//M05-2X/def2-TZVP level in the gas phase as well as in TCE, PhNO₂ and DMSO with the COSMO-RS solvation model.

	ΔE_{rel}^a	ΔG_{rel}^a			
		Gas	TCE	PhNO ₂	DMSO
1a	10.1	7.9	4.5 (−26.3)	3.1 (−26.8)	−2.0 (−36.4)
1b	7.3	4.8	0.6 (−27.1)	0.0 (−26.8)	−3.3 (−34.7)
1c	0.0	0.0	0.0 (−22.9)	0.0 (−22.0)	0.0 (−26.6)
1^{TS}	22.6	21.6	17.1 (−27.4)	15.4 (−28.2)	9.4 (−38.8)
2a	2.3	−1.0	−1.8 (−22.4)	−2.0 (−20.9)	−2.2 (−19.7)
2b	1.6	−1.5	−3.0 (−23.0)	−2.9 (−21.3)	−3.0 (−19.8)
2c	0.0	0.0	0.0 (−21.6)	0.0 (−19.9)	0.0 (−18.4)
2^{TS}	11.9	12.5	12.4 (−21.7)	12.2 (−20.1)	11.9 (−19.0)
	$\Delta E^{\ddagger b}$		$\Delta G^{\ddagger b}$		
1	22.6	21.6	17.1 (+1.0)	15.4 (−0.2)	12.7 (−0.6)
2	11.9	14.0	15.4 (0.0)	15.1 (−0.1)	14.9 (−0.4)
	$\Delta\Delta G_{\text{solv}}^{\text{rel} c}$	0.0	−4.5	−6.2	−12.2
	$\Delta\Delta G_{\text{solv}}^{\text{rel} d}$	0.0	−4.8	−6.7	−10.9

^a Relative to conformer **1c** for biphenyl **1**, and relative to conformer **2c** for biphenyl **2**. Absolute free energies of solvation in parentheses. ^b From equation 13; in parentheses: deviation from kinetic parameters determined experimentally. ^c Free solvation energy of transition state **1^{TS}** relative to doubly H-bonded conformer **1c**, calculated with the COSMO-RS solvation model and the COSMOtherm program. ^d From equation 16. All energy terms in kcal/mol.

would be a strong indicator of intramolecular hydrogen bonding in biphenyl **1**, more so than simple differences in chemical shifts at a given temperature.³⁷

In TCE and PhNO₂, as far as chemical shifts are concerned, the NH α nuclei of biphenyl **1**, that engage in intramolecular H-bonding, are strongly deshielded compared to the NH α nucleus of control arene **3** (by +1.12 and +1.79 ppm, respectively, see green and yellow series in Figure 7a as well as Table S2 in the SI section). This stands in contrast to the NH β nuclei that do not engage in such an interaction (−0.46 and −0.25 ppm in TCE and PhNO₂, respectively, see green and yellow series in Figure 7b and Table S2 in the SI section). NH α and NH β chemical shifts of doubly H-bonded biphenyl **1c** relative to reference scaffold **3** calculated by DFT methods using gauge-independent atomic orbitals in the gas phase were +1.6 and −1.0 ppm, respectively, in very good agreement with experimental data. Error sources are likely (1) the co-existence of doubly and singly H-bonded conformers in both solvents, and (2) specific solvent environments at the H α and H β sites.

Gradients measured for NH α in biphenyl **1** are markedly different from those of reference **3** in both TCE and PhNO₂ (relative gradients −6.7 vs −3.9 ppb/K, and −11.6 vs −7.0 ppb/K, respectively; see the slopes of the regression lines in Figure 7a and Table S2 in the SI section). To the contrary, differences in NH β gradients are much milder in both TCE and PhNO₂ (−5.1 vs −3.9 ppb/K and −7.1 vs −6.5 ppb/K, respectively).

In DMSO, chemical shifts of nuclei NH α in biphenyl **1** and control **3** are very similar (10.12 vs 10.27 ppm at 25 °C, see red series in Figure 7a and Table S2 in the SI section). Equally similar are chemical shifts of nuclei NH β (9.76 vs 9.81 ppm, see red series in Figure 7b). The corresponding gradients are almost identical

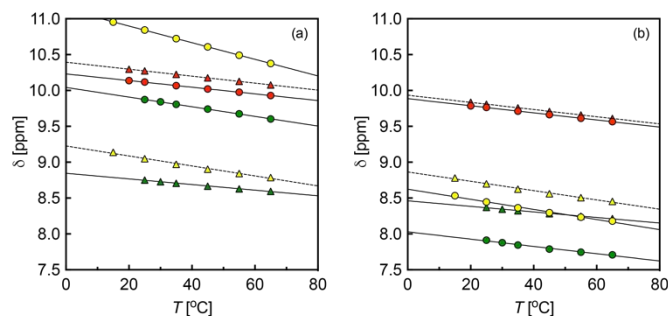


Figure 7. Chemical shifts of (a) hydrogens NH α and (b) NH β in biphenyl **1** (circles) and in reference phenyl hydrazide **3** (triangles) as a function of temperature. Solvents are TCE-d₂ (in green) in PhNO₂-d₅ (in yellow) and in DMSO-d₆ (in red). See Figure 1 for hydrogen numbering.

(−4.6 vs −4.9 ppb/K for nuclei NH α ; −5.0 ppb/K for NH β in both substrates). The near zero relative gradients suggest that intramolecular hydrogen bonding does not operate in DMSO, and would support structure **1a** as being the lowest energy ground state conformer. As shown above, calculations point to conformer **1b**, with a single intramolecular hydrogen bond, as the most stable ground state structure. While one could be tempted to dismiss *in silico* experiments, we note that (1) all functionals tested in this study, with and without correction for dispersive interactions, show conformer **1b** as the lowest energy ground state structure in DMSO, (2) none of these functionals would return correct free energies of torsion if conformer **1a** were the most stable conformer, and (3) extensive conformation screening unequivocally afforded conformer **1a** as the most stable structure without intramolecular hydrogen bonding. We suspect here that mono-H-bonded conformer **1b** is the most stable ground state structure, but that the strong solvation of the NH α H-bond donor by DMSO within the intramolecular hydrogen bond masks the impact of the latter on the chemical shifts and the gradients. We do acknowledge that the situation is ambiguous, however.

More than sixty years ago, Graybill and Leffler³⁸ showed that the free energies of torsion of a biphenyl unit bearing methoxy groups at its 2 and 2'-position and carboxamides at positions 6 and 6' are not significantly solvent-dependent (32.2 kcal/mol). However, enthalpy-entropy compensation was observed, with enthalpies of activation ranging from 21.5 to 30.6 kcal/mol and activation entropies from −29 to −7 cal/molK (see Figure 1 in ref. 14 for a plot of the compensation). Narrower ranges were measured when the carboxamides were replaced with COOCH₃ groups. In both cases, the authors could not identify any link between the nature of the solvent and the activation enthalpies (or entropies). A similar enthalpy-entropy compensation is observed here for biphenyl **2**, with increasing activation enthalpies and decreasing entropic penalties as the solvents become more polar (8.3 to 11.9 kcal/mol and −24 to −12 cal/molK from TCE to DMSO, see Table 2). A higher activation enthalpy accompanied by a weaker entropic penalty is also measured for biphenyl **1** when switching the solvent from TCE to PhNO₂ (9.0 vs 12.4 kcal/mol, and −24 vs −11 cal/molK, respectively; the ground state in DMSO is different, therefore

comparisons are irrelevant). A similar enthalpy-entropy compensation was very recently observed for amide bond rotations in 54 *N,N*-substituted arylamides bearing various aryl and amide substituents, all recorded in deuterated chloroform. While the free energy of rotation was 15.7 ± 0.2 kcal/mol on average, the range of activation enthalpies and entropies was impressive considering the structural similarities of the scaffolds (0.8 to 18.8 kcal/mol, and -46 to $+15$ cal/molK, respectively);³⁹ we suspect that solvation plays a major role in the compensation, but like all authors so far, we cannot rationalize these variations.

Accuracy, precision and limitations of the computational methods

We presented here computational data with the selection of functionals, basis sets and approximations that returned the torsional barriers closest to the experimental ones. Despite the remarkable accuracy of our calculated torsional barriers, error sources should still be discussed, as error compensation is a common occurrence. We identify at least six possible error sources: (1) the use of a limited number of ground and transition state conformers in our evaluation, (2) the type of functional and basis sets used in the gas phase optimization and the frequency calculations, (3) the higher level functional and basis sets used in single-point energy refinements, (4) the scaling (or non-scaling) of vibrational frequencies, (5) the possible refinement of the rigid rotor harmonic oscillator approximation to calculate the entropy contribution of low frequency vibrational normal modes, and (6) the parametrization of the method used to calculate solvation energies.

As far as error source (1) is concerned, barriers were also calculated using a larger set of possible conformers (8 ground states and 7 transition states), compared to just structures **1a** – **1c**, **1^{T5}**, **2a** – **2c** and **2^{T5}**. The error caused by using this smaller set (which is much easier to describe) is below 0.2 kcal/mol.

A clear trend emerges for error sources (2) and (3). Functionals tested in this study are presented in Table 3. Some were corrected with the D3(BJ)^{40,41} dispersive term. Ahlrichs basis sets def2-TZVP⁴² were used in all cases. Optimization and single-point energy refinement using functionals without a dispersive component severely underestimate the torsional barrier of biphenyl **1** (-2.4 , -1.9 and -1.1 kcal/mol in TCE, PhNO₂ and DMSO, respectively). This is likely due to an underestimation of the strength of the intramolecular hydrogen bonds in the ground state. To the contrary, when both functionals take into account dispersive interactions, the barrier is overestimated in TCE and PhNO₂ ($+1.9$ and $+1.3$ kcal/mol), and within 0.4 kcal/mol of experimental data in DMSO. This could suggest that dispersive terms overestimate the strength of the hydrogen bonds. The best combination in this case was to optimize structures with functionals uncorrected for dispersion, and to refine the energy with functionals that account for dispersion (average errors $+1.3$, $+0.4$ and -0.6 kcal/mol in TCE, PhNO₂ and DMSO, respectively). The B3LYP//M05-2X combination

afforded the most accurate barriers, as the M05-2X parametrization does account for some mid-range, dispersion-type interactions.^{43,44} It has also been shown to perform well in the calculation of barrier heights.^{25,45} Adding the explicitly dispersion-related term D3 to the M05-2X functional adds 1.2 kcal/mol to the free energies of torsion, which are then overestimated. This is likely due to some double counting of the dispersive interactions^{43,44} in the intramolecular hydrogen bonds. The trends in biphenyl **2** are not as pronounced (errors < 1.0 kcal/mol), but they are reversed. Also, we note that the typically highly accurate⁴⁴ double hybrid functionals DSD-PBEP86-D3(BJ) and DSD-BLYP-D3(BJ) do not improve the accuracy of the torsional barriers over the M05-2X functional in single point calculations.

Table 3. Functionals used for geometry optimization and single-point energy calculations, both in the gas phase. Basis sets are def2-TZVP.

Optimization	Single point calculations
TPSS ⁴⁶ -D3(BJ) ^{40,41}	M05-2X ²⁵ ; PW6B95 ⁴⁷ -D3(BJ); DSD-PBEP86 ⁴⁸ -D3(BJ)
B3LYP ⁴⁹ -D3(BJ)	
B3LYP	M05-2X; M05-2X-D3(0) ^{50,51} ; DSD-BLYP ⁵² -D3(BJ)
PBE0 ^{53,54}	M05-2X
BP ⁵⁵⁻⁵⁷	M05-2X

A scaling factor of 0.985 was used for vibrational frequencies computed with the B3LYP functional, while no scaling was applied to all other functionals (error source 4). The impact of scaling on the torsional barriers was insignificant (< 0.02 kcal/mol).

To address error source 5, we refined the entropic contributions of frequencies below 100 cm⁻¹ with the free-rotor approximation using Grimme's method.⁵⁸ However, very surprisingly, this refinement caused a significant underestimation across all tested functionals of the torsional barrier of biphenyl **2** (-1.8 vs -0.4 kcal/mol on average). The under- and overestimations of the biphenyl **1** barriers in the absence or presence of dispersion corrections were also exacerbated. The RRHO approximation, regardless of frequency, was thus chosen to better match experimental barriers. A controversial^{59,60} source of error could also be the use of vibrational frequencies calculated in the gas phase and not in solution (i.e. calculated in conjunction with a continuum solvation model). The alteration of vibrational degrees of freedom by the solvent and its impact on the entropic terms is thus neglected; however, Klamt and coworkers show that this effect is taken into account later when free energies of solvation are calculated using the COSMOtherm program.^{31,59}

As far as errors related to the solvation term are concerned (error source 6), the quality of the solvation free energies relies on the adequacy of the parametrization of the COSMOtherm program to evaluate our intramolecularly hydrogen bonded structures, a notoriously difficult task.^{44,58} We suspect that this uncertainty could be responsible for some of the unexpected trends described above. Overall, it is possible that our most accurate method (optimization and a strictly RRHO-based

vibrational analysis with the B3LYP functional, followed by single-point energy calculations with the M05-2X functional) benefits from some error cancellation after addition of the solvation term. In any case, for this pair of biphenyls, the method is highly accurate (mean deviation for both biphenyls **1** and **2** in all three solvents is -0.08 kcal/mol), and also very precise (root-mean-square deviation is 0.55 kcal/mol). We also attempted to replicate the impact of DMSO concentration in PhNO₂ on the torsional barrier of biphenyl **1**, by calculating with COSMOtherm the solvation energies of the lowest energy ground and transition states (structures **1b** and **1^{TS}**) in the 13 mixtures of PhNO₂ and DMSO presented in Figure 4. Outstanding accuracy was observed throughout the series, with errors consistently lower than 0.1 kcal/mol (see Table S1 in the SI section).

Conclusions

The fast and counterintuitive torsional isomerization of biphenyl **1** (at least at first sight) illustrates the multiple hurdles that hydrogen bonding interactions must face to provide extra stability to small molecules, supramolecular assemblies and larger entities such as proteins – and this even in non-aqueous environments. While the strength of the pair of intramolecular hydrogen bonds in conformer **1c** amounts to approximately 8 kcal/mol, polar solvents like PhNO₂, or polarizable ones like both TCE and PhNO₂, provide $5 - 6$ kcal/mol of additional stability to the separated hydrogen bond donors and acceptors at the transition state by a combination of dipole-dipole and dipole-induced dipole interactions between the solute and the solvent. As (1) the ground state conformation of biphenyl **2** (conformer **2b**) is less entropically penalizing than “wrapped” conformations **1c** and **2c** (a net gain of 1.5 kcal/mol), and (2) TCE and PhNO₂ solvate conformer **2b** slightly better than its transition state **2^{TS}** (by $1.1 - 1.4$ kcal/mol), the torsional barrier of biphenyl **1** is counterintuitively within 1 kcal/mol of that of reference biphenyl **2**. When the very strong hydrogen bond acceptor DMSO is used as solvent, at least one intramolecular hydrogen bond is disrupted in the ground state of biphenyl **1**, and the torsional barrier decreases further by approximately 3 kcal/mol compared to TCE. As a consequence, and again counterintuitively, biphenyl **1**, that is stabilized by one intramolecular hydrogen bond (see conformer **1b** in Figure 5) rotates along its C_{aryl}-C_{aryl} axis approximately 30 times faster than reference biphenyl **2** (see Figure 6), despite both of them being isosteric and ground state conformer **2b** mimicking the geometry of conformer **1b** perfectly.

Conflicts of interest

There are no conflicts to declare.

Acknowledgements

We are grateful to the National Science Foundation (grants CHE-1507321 and CHE-1905238), the American Chemical Society

Petroleum Research Fund (grant 56375-ND4), the Roenigk Family Foundation and Ohio University for their continuing financial support. HB is also supported by a fellowship from the Alfonso Martin Escudero Foundation. NK thanks the University of Strasbourg and the CNRS for financial support.

Notes and references

- P. A. Kollman and L. C. Allen, *Chem. Rev.*, 1972, **72**, 283–303.
- G. a. Jeffrey, *An Introduction to Hydrogen Bonding*, Oxford University Press, New York, 1997.
- S. J. Grabowski, *Chem. Rev.*, 2011, **111**, 2597–2625.
- E. Arunan, G. R. Desiraju, R. A. Klein, J. Sadlej, S. Scheiner, I. Alkorta, D. C. Clary, R. H. Crabtree, J. J. Dannenber, P. Hobza, H. G. Kjaergaard, A. C. Legon, B. Mennucci and D. J. Nesbitt, *Pure Appl. Chem.*, 2011, **83**, 1637–1641.
- T. Adachi and M. D. Ward, *Acc. Chem. Res.*, 2016, **49**, 2669–2679.
- M. M. Conn and J. Rebek, *Chem. Rev.*, 1997, **97**, 1647–1668.
- G. Cooke and V. M. Rotello, *Chem. Soc. Rev.*, 2002, **31**, 275–286.
- V. Amendola, L. Fabbrizzi and L. Mosca, *Chem. Soc. Rev.*, 2010, **39**, 3889–3915.
- D. González-Rodríguez and A. P. H. J. Schenning, *Chem. Mater.*, 2011, **23**, 310–325.
- D. Ajami, L. Liu and J. Rebek, *Chem. Soc. Rev.*, 2015, **44**, 490–499.
- L. Yang, X. Tan, Z. Wang and X. Zhang, *Chem. Rev.*, 2015, **115**, 7196–7239.
- S. K. Chang and A. D. Hamilton, *J. Am. Chem. Soc.*, 1988, **110**, 1318–1319.
- R. Joseph and E. Masson, *Org. Biomol. Chem.*, 2013, **11**, 3116–3127.
- E. Masson, *Org. Biomol. Chem.*, 2013, **11**, 2859–2871.
- R. Joseph and E. Masson, *Supramol. Chem.*, 2014, **26**, 632–641.
- R. Joseph and E. Masson, *Eur. J. Org. Chem.*, 2014, 105–110.
- C. A. Hunter, *Angew. Chem., Int. Ed.*, 2004, **43**, 5310–5324.
- B. S. Furniss, A. J. Hannaford, P. W. G. Smith and A. R. Tatchell, *Textbook of Practical Organic Chemistry*, Longman Scientific & Technical; John Wiley & Sons, Inc, Harlow, 5th edn., 1989.
- J. R. Rumble, *CRC handbook of chemistry and physics*, CRC Press, Boca Raton, FL, 100th edn., 2019.
- E. Ghera, Y. Gaoni and S. Shoua, *J. Am. Chem. Soc.*, 1976, **98**, 3627–3632.
- M. Casagrande, A. Barteselli, N. Basilico, S. Parapini, D. Taramelli and A. Sparatore, *Bioorg. Med. Chem.*, 2012, **20**, 5965–5979.
- S. Zhang, D. Zhang and L. S. Liebeskind, *J. Org. Chem.*, 1997, **62**, 2312–2313.
- K. Yasamut, J. Jongcharoenkamol, S. Ruchirawat and P. Ploypradith, *Tetrahedron*, 2016, **72**, 5994–6000.
- R. Cabot and C. A. Hunter, *Org. Biomol. Chem.*, 2010, **8**, 1943–1950.
- Y. Zhao, N. E. Schultz and D. G. Truhlar, *J. Chem. Theory Comput.*, 2006, **2**, 364–382.
- J. L. Cook, C. A. Hunter, C. M. R. Low, A. Perez-Velasco and J. G. Vinter, *Angew. Chem., Int. Ed.*, 2007, **46**, 3706–3709.
- J. L. Cook, C. A. Hunter, C. M. R. Low, A. Perez-Velasco and J. G. Vinter, *Angew. Chem., Int. Ed.*, 2008, **47**, 6275–6277.
- A. Klamt and G. Schüürmann, *J. Chem. Soc. Perkin Trans. 2*, 1993, 799–805.
- A. Klamt, *J. Phys. Chem.*, 1995, **99**, 2224–2235.
- A. Klamt, V. Jonas, T. Bürger and J. C. W. Lohrenz, *J. Phys. Chem. A*, 1998, **102**, 5074–5085.
- A. Hellweg and F. Eckert, *AIChE J.*, 2017, **63**, 3944–3954.

- 32 Eckert F, Klamt A. *COSMOtherm, Version C30, Release, 17.01. Leverkusen, Germany: COSMOlogic GmbH & Co. KG, 2016.*
- 33 Not tabulated; α_s value for tetrachloromethane used instead.
- 34 M. H. Abraham and J. A. Platts, *J. Org. Chem.*, 2001, **66**, 3484–3491.
- 35 J. Catalán and H. Hopf, *Eur. J. Org. Chem.*, 2004, 4694–4702.
- 36 SP value not tabulated, but based on the SP values of tetrachloromethane and 1,2-dichloroethane (both 0.77), see ref. 35.
- 37 T. Cierpicki and J. Otlewski, *J. Biomol. NMR*, 2001, **21**, 249–261.
- 38 B. M. Graybill and J. E. Leffler, *J. Phys. Chem.*, 1959, **63**, 1461–1463.
- 39 J. Guerra, B. Bajwa, P. Kumar, S. Vazquez, V. V. Krishnan and S. Maitra, *ACS Omega*, 2020, **5**, 9348–9355.
- 40 S. Grimme, J. Antony, S. Ehrlich and H. Krieg, *J. Chem. Phys.*, 2010, **132**, 154104.
- 41 S. Grimme, S. Ehrlich and L. Goerigk, *J. Comput. Chem.*, 2011, **32**, 1456–1465.
- 42 F. Weigend and R. Ahlrichs, *Phys. Chem. Chem. Phys.*, 2005, **7**, 3297–3305.
- 43 L. Goerigk, H. Kruse and S. Grimme, *ChemPhysChem*, 2011, **12**, 3421–3433.
- 44 L. Goerigk, A. Hansen, C. Bauer, S. Ehrlich, A. Najibi and S. Grimme, *Phys. Chem. Chem. Phys.*, 2017, **19**, 32184–32215.
- 45 Y. Zhao and D. G. Truhlar, *Theor. Chem. Acc.*, 2008, **120**, 215–241.
- 46 J. Tao, J. P. Perdew, V. N. Staroverov and G. E. Scuseria, *Phys. Rev. Lett.*, 2003, **91**, 146401.
- 47 Y. Zhao and D. G. Truhlar, *J. Phys. Chem. A*, 2005, **109**, 5656–5667.
- 48 S. Kozuch and J. M. L. Martin, *Phys. Chem. Chem. Phys.*, 2011, **13**, 20104–20107.
- 49 A. D. Becke, *J. Chem. Phys.*, 1993, **98**, 5648–5652.
- 50 Y. S. Lin, G. De Li, S. P. Mao and J. Da Chai, *J. Chem. Theory Comput.*, 2013, **9**, 263–272.
- 51 L. Goerigk, *J. Phys. Chem. Lett.*, 2015, **6**, 3891–3896.
- 52 S. Kozuch, D. Gruzman and J. M. L. Martin, *J. Phys. Chem. C*, 2010, **114**, 20801–20808.
- 53 M. Ernzerhof and G. E. Scuseria, *J. Chem. Phys.*, 1999, **110**, 5029–5036.
- 54 C. Adamo and V. Barone, *J. Chem. Phys.*, 1999, **110**, 6158–6170.
- 55 A. D. Becke, *Phys. Rev. A*, 1988, **38**, 3098–3100.
- 56 J. P. Perdew, *Phys. Rev. B*, 1986, **33**, 8822–8824.
- 57 J. P. Perdew, *Phys. Rev. B*, 1986, **34**, 7406.
- 58 S. Grimme, *Chem. - Eur. J.*, 2012, **18**, 9955–9964.
- 59 J. Ho, A. Klamt and M. L. Coote, *J. Phys. Chem. A*, 2010, **114**, 13442–13444.
- 60 R. F. Ribeiro, A. V. Marenich, C. J. Cramer and D. G. Truhlar, *J. Phys. Chem. B*, 2011, **115**, 14556–14562.